

# Enhanced Direction-Sensing Methods and Performance Analysis in Low-Altitude Wireless Network via a Rotation Antenna Array

Jinbing Jiang, Feng Shu, Minghao Chen, Jiatong Bai, Maolin Li, Yan Wang, Jiangzhou Wang

**Abstract**—Due to the directive property of each antenna element, the received signal power can be severely attenuated when the emitter deviates from the array boresight, which will lead to a severe degradation in sensing performance along the corresponding direction. Although existing rotatable array sensing methods such as recursive rotation root multiple signal classification (RR-Root-MUSIC) can mitigate this issue by iteratively rotating and sensing, several mechanical rotations and repeated eigendecomposition operations are required to yield a high computational complexity and low time-efficiency. To address this problem, a pre-rotation initialization with receive power as a rule is proposed to significantly reduce the computational complexity and improve the time-efficiency. Using this idea, a low-complexity enhanced direction-sensing framework with pre-rotation initialization and iterative greedy spatial-spectrum search (PRI-IGSS) is developed with three stages: (1) the normal vector of array is rotated to a set of candidates to find the optimal direction with the maximum sensing energy with the corresponding direction-of-arrival (DOA) value computed by the Root-MUSIC algorithm; (2) the array is mechanically rotated to the initial estimated direction and kept fixed; (3) an iterative greedy spatial-spectrum search or receiving beamforming method, motivated by reinforcement learning, is designed with a reduced search range and making a summation of all previous sampling variance matrices and the current one is adopted to provide an increasing performance gain as the iteration process continues. To assess the performance of the proposed method, the corresponding Cramer-Rao lower bound (CRLB) is derived with a simplified rotation model. Simulation results demonstrate that the proposed PRI-IGSS method performs much better than RR-Root-MUSIC and achieves the CRLB in term of mean squared error due to the fact there is no sample accumulation for the latter. Compared to the latter, the former also makes a significant reduction in computational complexity.

**Index Terms**—DOA, Rotatable array, Low-complexity, Pre-rotation.

With the rapid development of the low-altitude economy, unmanned aerial vehicles (UAVs) have gradually become an indispensable part of future wireless networks, enabling a wide range of applications from logistics distribution and emergency rescue to aerial inspection [1], [2], [3], [4]. For these practical low-altitude operations, real-time target monitoring is essential, particularly in millimeter-wave communication scenarios where rapid target mobility causes severe spatial tracking challenges [5], [6]. To address these challenges, accurate direction-of-arrival (DOA) estimation serves as a fundamental

enabler for precise spatial localization and beam alignment. Over the past decades, various DOA estimation techniques have been extensively investigated, primarily including conventional beamforming, maximum likelihood estimation, and high-resolution subspace-based algorithms. However, adapting these classical methods directly to highly dynamic and resource-constrained UAV networks remains a critical bottleneck.

Specifically, fully digital massive multiple-input multiple-output (MIMO) architectures provide maximum spatial degrees of freedom (DoF) but incur excessive hardware cost and power consumption, which are typically unbearable for light-load UAVs. While hybrid analog-digital (HAD) architectures have been widely adopted to alleviate these hardware burdens, conventional subspace-based DOA algorithms in both setups still face prohibitive computational complexity due to frequent eigenvalue decompositions (EVDs) [7], [8]. Although low-complexity estimators, such as rapid phase ambiguity elimination [9], multi-modal deep learning [10], and root multiple signal classification (Root-MUSIC) variants [11], have been proposed to reduce latency, their performance remains strictly bounded by the received signal-to-noise ratio (SNR). This limitation is particularly critical for UAVs equipped with fixed directional antennas: as the target moves away from the array boresight, the sensing precision drops rapidly due to severe energy losses [12]. Consequently, purely algorithmic improvements cannot fundamentally overcome the physical gain limitations of fixed array geometries.

To further overcome the physical limitations of fixed arrays, recent research has shifted towards reconfigurable array architectures and propagation environments. Movable antenna (MA) and fluid antenna systems gain spatial DoF by dynamically altering antenna positions [13], [14]. Specifically, MA systems can improve the received SNR by optimizing antenna positions [15], achieve precise null steering to suppress interference [16], and empower trajectory designs for efficient UAV data collection [17]. Meanwhile, fluid antennas redefine connectivity boundaries through flexible spatial sampling [18], [19]. This paradigm has been further extended to six-dimensional movable antennas [20], where joint position and orientation optimization enhances multi-access point coordination [21] and exploits statistical channel state information for broader spatial multiplexing [22]. In parallel, intelligent reflecting surfaces (IRS) have been introduced to reconfigure the wireless propagation environment [23], [24], thereby enhancing communication and sensing performance as well

Manuscript created October, 2020; This work was developed by the IEEE Publication Technology Department. This work is distributed under the L<sup>A</sup>T<sub>E</sub>X Project Public License (LPPL) ( <http://www.latex-project.org/> ) version 1.3. A copy of the LPPL, version 1.3, is included in the base L<sup>A</sup>T<sub>E</sub>X documentation of all distributions of L<sup>A</sup>T<sub>E</sub>X released 2003/12/01 or later. The opinions expressed here are entirely that of the author. No warranty is expressed or implied. User assumes all risk.

as physical-layer security. Recent studies have demonstrated the versatility of IRS in wireless systems. For example, IRS can enhance system DoF in low-rank channels [25], maximize secrecy rates in directional modulation networks through joint beamforming [26], [27], secure UAV communications via discrete phase shift designs [28], and ensure reliable target localization in dual-function radar communication systems [29], [30].

However, the current solutions are inadequate in addressing the issue of signal power attenuation caused by directional antennas when the UAV is in the null zone or the backside of the receiving array. The rotatable antenna (RA) array emerges as a more practical alternative [31]. By simply rotating the array mechanically, the main lobe can be physically aligned with the target, providing direct physical-layer array gains and enhanced spatial resolution without the need for complex internal array reconfiguration [32]. For instance, rotatable antenna arrays have been shown to significantly improve hybrid precoding performance for UAV millimeter-wave communications by mechanically tracking users [33].

While RAs offer distinct physical gain advantages, existing methods like recursive rotation Root-MUSIC (RR-Root-MUSIC) [34] heavily rely on repeated mechanical rotations and full-scale EVDs, inducing substantial overhead and unacceptable sensing delays for highly mobile UAVs. To resolve this critical bottleneck, a novel pre-rotation initialization and iterative greedy spatial-spectrum search (PRI-IGSS) scheme is proposed in this paper. Instead of recursive physical scanning, PRI-IGSS utilizes a limited number of mechanical rotations to coarsely align the high-gain beam and obtains an initial estimate via Root-MUSIC. Subsequently, the array is rotated to keep the target within the main lobe, and the sensing precision is iteratively refined in the digital domain through a greedy local search. In this way, the proposed method preserves the physical gain of RAs while drastically reducing mechanical rotation overhead and computational latency, making it highly suitable for real-time UAV target tracking. The main contributions of this paper can be summarized as follows:

- 1) To tackle the severe signal attenuation caused by the directive pattern of antenna elements, a rotatable array direction-sensing system model is established. By rotating the array toward the target, it can effectively ease the problem of sensing performance degradation particularly when the emitter deviates from the array boresight. Furthermore, based on this model, the corresponding Cramer-Rao lower bound (CRLB) is derived by virtue of statistical theory and matrix analysis, which provides a theoretical benchmark to evaluate the following direction-sensing methods.
- 2) To achieve a high-precision direction-sensing performance with low-complexity, a PRI is proposed. First, the array is rotated to a set of candidate angles, which is equi-spaced rotation or sampling along elevation and azimuth to find the optimal direction with the maximum received power, and an initial direction is estimated by the Root-MUSIC algorithm. Subsequently, the array is rotated to this sensed direction and kept to be fixed. Finally, an IGSS is iteratively performed as the search

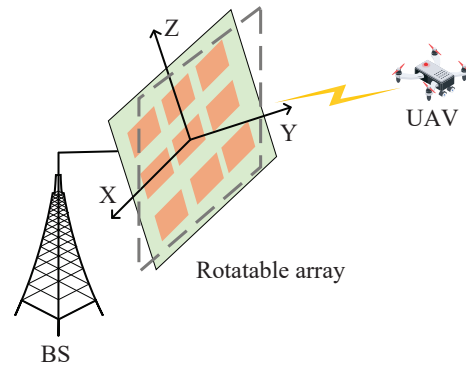


Fig. 1. rotatable array system for low-altitude communication network.

range is reduced gradually, and the sensing precision grows gradually with a continuous sampled signal accumulation process, which sum up to the current sampling variance matrix including all previous ones in the current round. Here, CRLB is utilized to design the search step-size. The proposed method makes a great sensing performance improvement over the conventional RR-Root-MUSIC and proposed PRI during the summation of sampling variance matrices. Their computational complexities are in decreasing order as follows: RR-Root-MUSIC, PRI-IGSS, and PRI.

- 3) In accordance with simulation results, the proposed PRI-IGSS method can achieve the corresponding CRLB. More important, by exploiting a continuous sample accumulation mechanism, the performance of the proposed method is significantly improved compared to the traditional non-memory RR-Root-MUSIC. Specifically, across the entire SNR and angular domains, an achievable performance gain of approximately one order of magnitude over RR-Root-MUSIC is consistently maintained. Furthermore, in extreme off-boresight scenarios, e.g.,  $\theta > 80^\circ$ , the proposed PRI and PRI-IGSS exhibit tremendous spatial robustness; while conventional FA (fixed array)-Root-MUSIC suffers severe degradation, resulting in a massive error gap of up to three and four orders of magnitude, the proposed PRI-IGSS remains highly reliable and accurate. Additionally, an optimal pre-rotation configuration of  $Q = 3$  is verified to perfectly balance the array high-gain coverage and the system overhead.

The remainder of this research is organized as follows. The system model of rotatable array is described in Section II. In Section III, the corresponding CRLB is also derived. In Section IV, two methods, PRI and PRI-IGR, are proposed. Moreover, section V presents the experimental results, with conclusions provided in Section VII.

## I. SYSTEM MODEL

As shown in Fig. 1, a rotatable array system for low-altitude communication network is considered where UAV is equipped with a single isotropic fixed antenna. The base station (BS) is equipped with a rotatable uniform planar array (UPA), which is

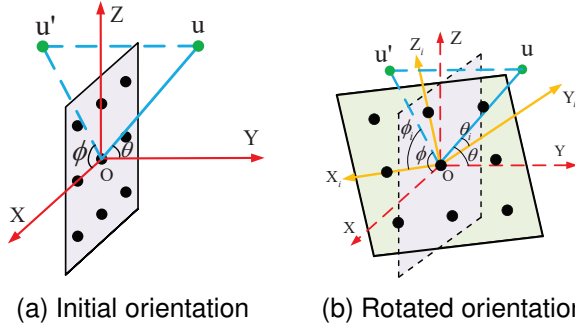


Fig. 2. Illustration of the geometric relationship for the rotatable array and emitter.

composed of directional antennas. Without loss of generality, the array is deployed on the  $x$ - $z$  plane of a three-dimensional (3D) Cartesian coordinate system with the origin as the center, and its size is  $M \times N$ , where  $M$  and  $N$  represent the number of antennas along the  $x$ -axis and  $z$ -axis, respectively. The separations between adjacent antennas in two axes are denoted by  $d_x$  and  $d_z$ , respectively. Therefore, the whole UPA size can be expressed as  $Md_x \times Nd_z$ .

For convenience, assuming that both  $M$  and  $N$  are odd numbers, the  $(m, n)$ -th antenna is located at the  $m$ -th column ( $m = 0, \dots, M-1$ ) and  $n$ -th row ( $n = 0, \dots, N-1$ ) on the UPA, which can be written as

$$\mathbf{p}_{m,n} = [x_m, 0, z_n]^T, \quad (1)$$

where  $x_m = (m - \frac{M-1}{2})d_x$  and  $z_n = (n - \frac{N-1}{2})d_z$ .

Fig. 2 illustrates the geometric relationships for the rotatable array and emitter. The angle  $\theta$  between the emitter direction and the  $y$ -axis, and  $\phi$  between the projection of the emitter direction onto the  $x$ - $z$  plane and the  $x$ -axis, are denoted as the elevation and azimuth angles of the UAV with respect to the origin of the coordinate system, respectively. Accordingly, the unit direction vector of the emitter is shown as

$$\begin{aligned} \mathbf{u} &= [u_x, u_y, u_z]^T \\ &= [\sin \theta \cos \phi, \cos \theta, \sin \theta \sin \phi]^T, \end{aligned} \quad (2)$$

where  $\theta \in [0, \pi]$  and  $\phi \in [-\pi, \pi]$ .

Hence, the array manifold is given by

$$\mathbf{a}(\theta, \phi) = \mathbf{a}_z(u_z) \otimes \mathbf{a}_x(u_x), \quad (3)$$

where

$$\mathbf{a}_z(u_z) = \begin{bmatrix} e^{j\frac{2\pi}{\lambda}z_0u_z} \\ \dots \\ e^{j\frac{2\pi}{\lambda}z_nu_z} \\ \dots \\ e^{j\frac{2\pi}{\lambda}z_{N-1}u_z} \end{bmatrix}, \quad \mathbf{a}_x(u_x) = \begin{bmatrix} e^{j\frac{2\pi}{\lambda}x_0u_x} \\ \dots \\ e^{j\frac{2\pi}{\lambda}x_mu_x} \\ \dots \\ e^{j\frac{2\pi}{\lambda}x_{M-1}u_x} \end{bmatrix}. \quad (4)$$

According to [31], the general antenna directional gain pattern is defined as

$$G(\varphi) = \begin{cases} G_0 \cos^{2p}(\varphi), & \varphi \in [0, \frac{\pi}{2}] \\ 0, & \text{otherwise,} \end{cases} \quad (5)$$

where  $\varphi$  is the boresight deflection angle between the emitter direction and the normal vector of the array,  $G_0 = 2(2p+1)$

is the maximum gain in the normal direction (i.e.,  $\varphi = 0$ ) that meets the law of power conservation.

Considering that each element has the same antenna pattern and the free-space propagation path loss, the channel amplitude gain between the UAV and the BS is modeled as

$$g(\varphi) = \begin{cases} \sqrt{\frac{A}{4\pi r^2}} G(\varphi), & \varphi \in [0, \frac{\pi}{2}] \\ 0, & \text{otherwise,} \end{cases} \quad (6)$$

where the integral space  $A$  corresponds to the surface region of rotatable array, and  $r$  is the distance between emitter and array.

To simplify, a constant is defined as  $g_0 = \sqrt{\frac{A}{4\pi r^2}} G_0$ . Substituting Eq. (5) into Eq. (6), the effective channel gain is rewritten as

$$g(\varphi) = \begin{cases} g_0 \cos^p(\varphi), & \varphi \in [0, \frac{\pi}{2}] \\ 0, & \text{otherwise.} \end{cases} \quad (7)$$

Assume that the signal  $s$ , emitted by the UAV, is a narrowband signal, and  $\mathbb{E}\{s^2\} = P_t$ . Let  $\mathbf{y} \in \mathbb{C}^{MN \times 1}$  be the received data vector as follows

$$\mathbf{y} = s g(\varphi) \mathbf{a}(\theta, \phi) + \mathbf{n}, \quad (8)$$

where  $\mathbf{n} \sim \mathcal{CN}(0, \sigma^2 \mathbf{I})$  is the additive white Gaussian noise (AWGN) vector.

Correspondingly, the received signal at the  $(m, n)$ -th antenna can be expressed as

$$y_{m,n} = s g(\varphi) e^{j\frac{2\pi}{\lambda}(x_m u_x + z_n u_z)} + n_{m,n}, \quad (9)$$

where  $\lambda$  is the wavelength and  $n_{m,n}$  denotes the AWGN of the  $(m, n)$ -th antenna.

In Fig. 2(a), the rotation array is placed on the  $x$ - $z$  plane. Therefore, the normal vector of array is aligned with the  $y$ -axis which is expressed as

$$\overrightarrow{OY_0} = [0, 1, 0]^T. \quad (10)$$

In accordance with the well-known cosine identity [35], the boresight deflection angle  $\varphi$  is

$$\varphi = \theta. \quad (11)$$

Now, let us consider the rotatable array model. The mechanical 3D rotation of the array is denoted by a rotation matrix  $\mathbf{R} \in \mathbb{R}^{3 \times 3}$ . Assuming the local coordinate system rotates synchronously with the array, the direction vector of the emitter in the local frame after rotation is given by

$$\mathbf{u}_l = \mathbf{R}^T \mathbf{u} = [u_{l,x}, u_{l,y}, u_{l,z}]^T. \quad (12)$$

Based on this local coordinate system, the local boresight deflection angle becomes  $\varphi_l = \theta_l = \arccos(u_{l,y})$ . Consequently, the received signal at the  $(m, n)$ -th antenna after rotation is expressed as

$$y_{l,m,n} = s g(\theta_l) e^{j\frac{2\pi}{\lambda}(x_m u_{l,x} + z_n u_{l,z})} + n_{m,n}. \quad (13)$$

## II. DERIVED CRLB FOR ROTATABLE ARRAY

To evaluate the performance of the proposed methods, the CRLB for the rotatable array is derived as a theoretical benchmark [36], [37]. For notational simplicity, the elevation and azimuth angles in the rotated coordinate system are simply denoted as  $(\theta, \phi)$  in the following derivation.

Based on the received signal model in Eq. (13), the observation at the  $(m, n)$ -th antenna element can be equivalently rewritten by separating the deterministic component and the noise, given by

$$\tilde{y}_{m,n} = \tilde{\mu}_{m,n} + n_{m,n}, \quad (14)$$

where the deterministic signal part  $\tilde{\mu}_{m,n}$  is defined as

$$\tilde{\mu}_{m,n} = s g(\theta) e^{j\psi_{m,n}(\theta, \phi)}, \quad (15)$$

and the corresponding phase term is

$$\begin{aligned} \psi_{m,n}(\theta, \phi) &= \frac{2\pi}{\lambda} (x_m u_x + z_n u_z) \\ &= \frac{2\pi}{\lambda} (x_m \sin \theta \cos \phi + z_n \sin \theta \sin \phi). \end{aligned} \quad (16)$$

The corresponding received signal vector of BS is

$$\tilde{\mathbf{y}} = [\tilde{y}_{0,0}, \tilde{y}_{0,1}, \dots, \tilde{y}_{M-1, N-1}]^T. \quad (17)$$

Let us define the parameter vector as follows

$$\boldsymbol{\theta} = [\theta, \phi]^T. \quad (18)$$

Referring to [38], the likelihood function of  $\tilde{\mathbf{y}}$  is given by

$$p(\tilde{\mathbf{y}}; \boldsymbol{\theta}) = (\pi\sigma^2)^{-MN} \exp\left(-\frac{\|\tilde{\mathbf{y}} - \boldsymbol{\mu}(\boldsymbol{\theta})\|^2}{\sigma^2}\right), \quad (19)$$

where  $\boldsymbol{\mu}(\boldsymbol{\theta})$  denotes the deterministic mean vector.

In order to derive the joint CRLB for the elevation and azimuth angles, the Fisher information matrix (FIM) [39] is defined as

$$[\mathbf{F}(\boldsymbol{\theta})]_{ij} = -E \left[ \frac{\partial^2 \ln p(\tilde{\mathbf{y}}; \boldsymbol{\theta})}{\partial \theta_i \partial \theta_j} \right]. \quad (20)$$

Furthermore, Eq. (20) is simplified as

$$[\mathbf{F}(\boldsymbol{\theta})]_{ij} = \frac{2}{\sigma^2} \sum_{m=0}^{M-1} \sum_{n=0}^{N-1} \Re \left\{ \frac{\partial \tilde{\mu}_{m,n}}{\partial \theta_i} \cdot \frac{\partial \tilde{\mu}_{m,n}^*}{\partial \theta_j} \right\}, \quad (21)$$

where

$$\begin{aligned} &\Re \left\{ \left( \frac{\partial \tilde{\mu}_{m,n}}{\partial \boldsymbol{\theta}} \right) \left( \frac{\partial \tilde{\mu}_{m,n}}{\partial \boldsymbol{\theta}} \right)^H \right\} \\ &= s^2 \begin{bmatrix} \left( \frac{\partial g(\theta)}{\partial \theta} \right)^2 + g^2(\theta) \left( \frac{\partial \psi_{m,n}}{\partial \theta} \right)^2 & g^2(\theta) \frac{\partial \psi_{m,n}}{\partial \theta} \frac{\partial \psi_{m,n}}{\partial \phi} \\ g^2(\theta) \frac{\partial \psi_{m,n}}{\partial \theta} \frac{\partial \psi_{m,n}}{\partial \phi} & g^2(\theta) \left( \frac{\partial \psi_{m,n}}{\partial \phi} \right)^2 \end{bmatrix}. \end{aligned} \quad (22)$$

Differentiating  $\psi_{m,n}$  with respect to  $\theta$  and  $\phi$  based on Eq. (16) yields

$$\frac{\partial \psi_{m,n}}{\partial \theta} = k \cos \theta (x_m \cos \phi + z_n \sin \phi), \quad (23)$$

and

$$\frac{\partial \psi_{m,n}}{\partial \phi} = k \sin \theta (-x_m \sin \phi + z_n \cos \phi), \quad (24)$$

where  $k = \frac{2\pi}{\lambda}$ .

Since  $M$  and  $N$  are odd numbers and the array elements are symmetrically distributed, we have  $\sum_{m,n} x_m = 0$ ,  $\sum_{m,n} z_n = 0$ ,  $\sum_{m,n} x_m z_n = 0$ . Let us define

$$\begin{aligned} S_m &= \sum_{m=0}^{M-1} x_m^2 = \frac{M(M^2-1)}{12} d_x^2, \\ S_n &= \sum_{n=0}^{N-1} z_n^2 = \frac{N(N^2-1)}{12} d_z^2. \end{aligned} \quad (25)$$

Consequently, the single-snapshot FIM is derived as

$$\mathbf{F}_{(1 \text{ snap})}(\boldsymbol{\theta}) = \frac{2s^2}{\sigma^2} \begin{bmatrix} P & Q \\ Q & R \end{bmatrix}, \quad (26)$$

where

$$\begin{aligned} P &= MN \left( \frac{\partial g(\theta)}{\partial \theta} \right)^2 \\ &\quad + (kg(\theta) \cos \theta)^2 [MS_n \sin^2 \phi + NS_m \cos^2 \phi], \\ Q &= (kg(\theta))^2 \sin \theta \cos \theta \sin \phi \cos \phi [MS_n - NS_m], \\ R &= (kg(\theta) \sin \theta)^2 [MS_n \cos^2 \phi + NS_m \sin^2 \phi]. \end{aligned} \quad (27)$$

Given  $K$  independent measurements  $\mathbf{y}[1], \dots, \mathbf{y}[K]$ , the total FIM is expressed as

$$\mathbf{F}(\boldsymbol{\theta}) = \frac{2Ks^2}{\sigma^2} \begin{bmatrix} P & Q \\ Q & R \end{bmatrix}. \quad (28)$$

Differentiating Eq. (7) with respect to  $\theta$  yields

$$\frac{\partial g(\theta)}{\partial \theta} = -g_0 p \cos^{p-1} \theta \sin \theta. \quad (29)$$

By substituting Eq. (29) into Eq. (27), the elements of the FIM are reformulated as

$$\begin{aligned} P &= MN (g_0 p \cos^{p-1} \theta \sin \theta)^2 \\ &\quad + (kg_0 \cos^{p+1} \theta)^2 [MS_n \sin^2 \phi + NS_m \cos^2 \phi], \\ Q &= (kg_0 \cos^p \theta)^2 \sin \theta \cos \theta \sin \phi \cos \phi [MS_n - NS_m], \\ R &= (kg_0 \cos^p \theta \sin \theta)^2 [MS_n \cos^2 \phi + NS_m \sin^2 \phi]. \end{aligned} \quad (30)$$

Therefore, the CRLB matrix is obtained by inverting the FIM, expressed as

$$\text{CRLB} = \mathbf{F}^{-1}(\boldsymbol{\theta}) = \frac{\sigma^2}{2Ks^2(PR-Q^2)} \begin{bmatrix} R & -Q \\ -Q & P \end{bmatrix}. \quad (31)$$

Let  $\gamma = \frac{2Ks^2}{\sigma^2}$  denote the received SNR at the array. The closed-form expressions of the theoretical lower bounds are subsequently derived as Eq. (32) and Eq. (33).

As indicated by Eq. (32) and Eq. (33), the estimation performance is severely constrained by the directional antenna gain. When the target is aligned with the array boresight (i.e.,  $\theta \approx 0$ ), the antenna gain is maximized, yielding the minimum CRLB. Conversely, as the signal direction deviates from the normal vector, the effective SNR is significantly attenuated by the rapidly decreasing gain, which causes a sharp increase in the CRLB and a severe degradation in estimation accuracy. To overcome the performance loss outside the high-gain region, the array orientation must be mechanically adjusted to steer the target direction. This critical requirement directly motivates the pre-rotation initialization strategy proposed in the following section.

$$\text{CRLB}_\theta(\theta, \phi) = \frac{\frac{1}{\gamma}(MS_n \cos^2 \phi + NS_m \sin^2 \phi)}{MN g_0^2 \left[ p^2 \cos^{2p-2} \theta \sin^2 \theta (MS_n \cos^2 \phi + NS_m \sin^2 \phi) + k^2 \cos^{2p+2} \theta S_m S_n \right]}. \quad (32)$$

$$\text{CRLB}_\phi(\theta, \phi) = \frac{\frac{1}{\gamma} \left( MN p^2 \cos^{2p-2} \theta \sin^2 \theta + k^2 \cos^{2p+2} \theta (MS_n \sin^2 \phi + NS_m \cos^2 \phi) \right)}{MN g_0^2 k^2 \cos^{2p} \theta \sin^2 \theta \left[ p^2 \cos^{2p-2} \theta \sin^2 \theta (MS_n \cos^2 \phi + NS_m \sin^2 \phi) + k^2 \cos^{2p+2} \theta S_m S_n \right]}. \quad (33)$$

### III. PROPOSED LOW-COMPLEXITY ROTATABLE ARRAY DOA METHODS

In this section, to reduce the high complexity and enhance the estimation performance, a low-complexity DOA method is proposed. As illustrated in Fig. 3, the proposed framework consists of three main steps: PRI is proposed in first subsection, rotating the array to the initial estimate direction, and IGSS is proposed in second subsection. Finally, a detailed computational complexity analysis is presented.

#### A. Proposed Low-Complexity PRI Method

As the emitter deviates from the array boresight, the array gain decreases rapidly due to the directive antenna pattern, causing a severe attenuation in the received SNR and a consequent degradation in estimation accuracy. To overcome this limitation, a low-complexity PRI method is introduced in this subsection. Specifically, the array orientation is coarsely adjusted to an optimal direction with the maximum received power, thereby significantly enhancing the effective SNR.

Specifically, the array is rotated around the  $z$ -axis and the  $x$ -axis. The discrete candidate scanning angle sets for these rotations are defined as

$$\Psi_\alpha = \{\alpha_1, \dots, \alpha_Q\}, \quad (34)$$

$$\Psi_\beta = \{\beta_1, \dots, \beta_Q\}, \quad (35)$$

where  $\Psi_\alpha$  and  $\Psi_\beta$  correspond to the rotation angles around the  $z$ -axis and the  $x$ -axis, respectively, and  $Q$  denotes the number of uniformly distributed angles in each dimension.

For a specific pair of candidate angles  $(\alpha_i, \beta_j)$ , the elementary rotation matrices are given by

$$\mathbf{R}_z(\alpha_i) = \begin{bmatrix} \cos \alpha_i & -\sin \alpha_i & 0 \\ \sin \alpha_i & \cos \alpha_i & 0 \\ 0 & 0 & 1 \end{bmatrix}, \quad (36)$$

$$\mathbf{R}_x(\beta_j) = \begin{bmatrix} 1 & 0 & 0 \\ 0 & \cos \beta_j & -\sin \beta_j \\ 0 & \sin \beta_j & \cos \beta_j \end{bmatrix}. \quad (37)$$

The combined 3D rotation matrix is expressed as

$$\mathbf{R}(\alpha_i, \beta_j) = \mathbf{R}_z(\alpha_i) \mathbf{R}_x(\beta_j). \quad (38)$$

By traversing all combinations of candidate directions, a pre-rotation candidate set comprising  $Q^2$  orientations is constructed as

$$\Omega = \{\mathbf{R}_q \mid \mathbf{R}_q = \mathbf{R}(\alpha_i, \beta_j), \forall \alpha_i \in \Psi_\alpha, \beta_j \in \Psi_\beta\}, \quad (39)$$

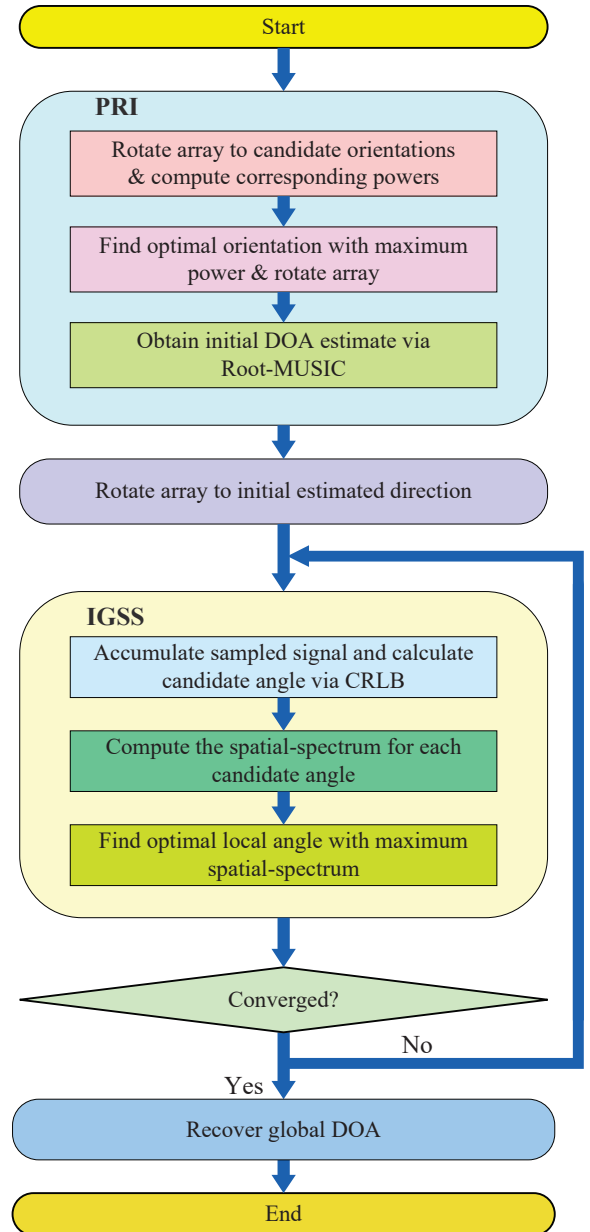


Fig. 3. Flowchart of the proposed low-complexity enhanced direction-sensing method via a rotatable antenna array.

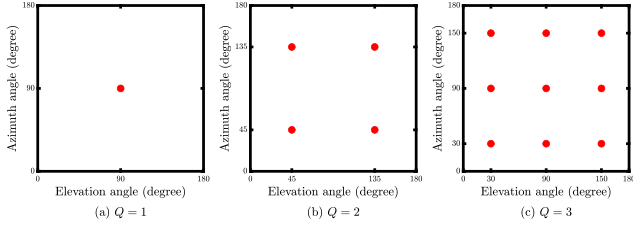


Fig. 4. Illustration of the spatial distribution of the different pre-rotation candidate set  $\Omega$ .

where  $q = 1, 2, \dots, Q^2$  is the index of the candidate orientations.

Since  $Q$  is deliberately set to a small integer for coarse initialization, the size of the search space is significantly constrained, which theoretically guarantees the low computational complexity of the PRI stage.

To demonstrate the pre-rotation process, Fig. 4 illustrates the spatial distribution of the pre-rotation candidate set  $\Omega$ . It can be observed that as  $Q$  increases, the points within the candidate set  $\Omega$  become denser, thereby providing finer coverage of high-gain search directions within the given fixed angular range.

For each candidate orientation  $\mathbf{R}_q \in \Omega$ , the received signal is collected over  $K$  snapshots. The corresponding received power is computed as

$$P(\mathbf{R}_q) = \sum_{k=1}^K \|\mathbf{y}_q[k]\|_2^2, \quad (40)$$

where  $\mathbf{y}_q[k]$  denotes the  $k$ -th snapshot of the received signal vector defined in Eq. (8) under the  $q$ -th orientation.

The optimal rotation matrix, denoted as  $\mathbf{R}^*$ , is determined by maximizing the received power as follows

$$\mathbf{R}^* = \arg \max_{\mathbf{R}_q \in \Omega} P(\mathbf{R}_q). \quad (41)$$

Subsequently, the array is mechanically rotated to this optimal direction. Based on the optimally rotated array, the sample covariance matrix of the received signal is calculated as

$$\hat{\mathbf{R}}_{yy} = \frac{1}{K} \sum_{k=1}^K \mathbf{y}[k] \mathbf{y}^H[k], \quad (42)$$

where  $\mathbf{y}[k]$  is the received signal at the  $k$ -th snapshot.

Finally, the EVD of  $\hat{\mathbf{R}}_{yy}$  is performed as

$$\hat{\mathbf{R}}_{yy} = [\hat{\mathbf{U}}_s, \hat{\mathbf{U}}_n] \mathbf{\Sigma} [\hat{\mathbf{U}}_s, \hat{\mathbf{U}}_n]^H, \quad (43)$$

where  $\mathbf{\Sigma}$  is the diagonal matrix of eigenvalues,  $\hat{\mathbf{U}}_s = [\hat{\mathbf{u}}_1] \in \mathbb{C}^{MN \times 1}$  is the estimated signal subspace, and  $\hat{\mathbf{U}}_n = [\hat{\mathbf{u}}_2, \dots, \hat{\mathbf{u}}_{MN}] \in \mathbb{C}^{MN \times (MN-1)}$  is the estimated noise subspace.

Based on the MUSIC principle, the array manifold vector is orthogonal to the noise subspace. Thus, the spatial cost function of the 2D-MUSIC algorithm is formulated as

$$\mathcal{J}(\boldsymbol{\theta}) = \sum_{i=2}^{MN} |\hat{\mathbf{u}}_i^H (\mathbf{a}_z(u_z) \otimes \mathbf{a}_x(u_x))|^2. \quad (44)$$

To avoid an exhaustive 2D search and reduce computational complexity, the noise eigenvector is reshaped into a matrix  $\hat{\mathbf{N}}_i \in \mathbb{C}^{MN \times N}$  such that  $\hat{\mathbf{u}}_i = \text{vec}(\hat{\mathbf{N}}_i)$ . Consequently, the cost function in Eq. (44) is rewritten as

$$\begin{aligned} \mathcal{J}(\boldsymbol{\theta}) &= \sum_{i=2}^{MN} \left| \mathbf{a}_x^H(u_x) \hat{\mathbf{N}}_i^H \mathbf{a}_z(u_z) \right|^2 \\ &= \mathbf{a}_x^H(u_x) \left( \sum_{i=2}^{MN} \hat{\mathbf{N}}_i (\mathbf{a}_z(u_z) \mathbf{a}_z^H(u_z)) \hat{\mathbf{N}}_i^H \right) \mathbf{a}_x(u_x). \end{aligned} \quad (45)$$

By substituting the approximation  $\mathbf{a}_z(u_z) \mathbf{a}_z^H(u_z) \approx \mathbf{I}_N$  into (45), the original 2D coupled problem is decoupled into two independent 1D Root-MUSIC problems. The decoupled cost function for the  $x$ -dimension is given by

$$\mathcal{J}_x(u_x) = \mathbf{a}_x^H(u_x) \left( \sum_{i=2}^{MN} \hat{\mathbf{N}}_i \hat{\mathbf{N}}_i^H \right) \mathbf{a}_x(u_x). \quad (46)$$

Similarly, the cost function for the  $z$ -dimension is decoupled as

$$\mathcal{J}_z(u_z) = \mathbf{a}_z^H(u_z) \left( \sum_{i=2}^{MN} \hat{\mathbf{N}}_i^H \hat{\mathbf{N}}_i \right) \mathbf{a}_z(u_z). \quad (47)$$

In accordance with Eq. (46) and Eq. (47), the local direction cosines  $\hat{u}_x$  and  $\hat{u}_z$  are independently estimated. Subsequently, the local elevation and azimuth angles are reconstructed as

$$\hat{\theta}_l = \arccos \left( \sqrt{1 - \hat{u}_z^2 - \hat{u}_x^2} \right), \quad (48)$$

$$\hat{\phi}_l = \text{atan2}(\hat{u}_z, \hat{u}_x). \quad (49)$$

Let  $\hat{\mathbf{u}}_l$  denote the local direction vector constructed from these local angles. The initial global direction vector is recovered by mapping it back to the global coordinate system via the previously selected optimal rotation matrix  $\mathbf{R}^*$ :

$$\hat{\mathbf{u}}_{\text{init}} = \mathbf{R}^* \hat{\mathbf{u}}_l. \quad (50)$$

Finally, the initial global DOA estimate  $\hat{\boldsymbol{\theta}}_{\text{init}}$  is extracted from the elements of  $\hat{\mathbf{u}}_{\text{init}}$  using the inverse trigonometric mapping defined in Eq. (48) and Eq. (49).

### B. Proposed Low-Complexity IGSS Method

In this stage, an IGSS method is introduced to further enhance the estimation accuracy through an iterative greedy search and continuous snapshot accumulation.

Based on the initial global direction estimate  $\hat{\mathbf{u}}_{\text{init}} = [\hat{u}_{\text{init},x}, \hat{u}_{\text{init},y}, \hat{u}_{\text{init},z}]^T$ , the mechanical rotation angles required to align the array boresight with the target are computed as

$$\alpha_{\text{init}} = \text{atan2}(-\hat{u}_{\text{init},x}, \hat{u}_{\text{init},y}), \quad (51)$$

$$\beta_{\text{init}} = \arcsin(\hat{u}_{\text{init},z}). \quad (52)$$

Then the corresponding rotation matrix is given by

$$\mathbf{R}_{\text{init}} = \mathbf{R}_z(\alpha_{\text{init}}) \mathbf{R}_x(\beta_{\text{init}}). \quad (53)$$

The array is mechanically rotated to the initial direction using  $\mathbf{R}_{\text{init}}$  and keeps fixed for the remainder of the estimation process.

Since the array normal vector has been aligned with the initial global estimate  $\hat{\mathbf{u}}_{\text{init}}$  via mechanical rotation, the initial local DOA estimate in the rotated coordinate system is naturally set as the origin, i.e.,

$$\hat{\boldsymbol{\theta}}_{l,0} = [0, 0]^T. \quad (54)$$

This initialization serves as the starting point for the subsequent greedy search process.

Under this fixed orientation, the spatial spectrum is evaluated in the local coordinate system. For any candidate local direction  $\boldsymbol{\theta}_l = [\theta_l, \phi_l]^T$ , the local direction vector is denoted as  $\mathbf{u}_l(\theta_l, \phi_l)$ . Consequently, the corresponding local steering vector  $\mathbf{a}(\boldsymbol{\theta}_l)$  is directly constructed as

$$\mathbf{a}(\boldsymbol{\theta}_l) = \left[ e^{j\frac{2\pi}{\lambda} \mathbf{P}_{0,0}^T \mathbf{u}_l}, \dots, e^{j\frac{2\pi}{\lambda} \mathbf{P}_{M-1,N-1}^T \mathbf{u}_l} \right]^T. \quad (55)$$

Assuming the array continuously collects snapshots. Let  $\mathbf{Y}_i \in \mathbb{C}^{MN \times K}$  denote the new snapshot matrix collected during the  $i$ -th iteration stage. The accumulated data matrix up to  $i$ -th iteration is defined as

$$\mathbf{Y}^{(i)} = [\mathbf{Y}_1, \dots, \mathbf{Y}_i] \in \mathbb{C}^{MN \times iK}. \quad (56)$$

The corresponding sample covariance matrix is calculated by

$$\hat{\mathbf{R}}_{yy}^{(i)} = \frac{1}{iK} \mathbf{Y}^{(i)} \left( \mathbf{Y}^{(i)} \right)^H. \quad (57)$$

To circumvent the computational burden of directly computing the covariance matrix from scratch,  $\hat{\mathbf{R}}_{yy}^{(i)}$  is equivalently updated in a recursive manner as follows

$$\hat{\mathbf{R}}_{yy}^{(i)} = \frac{i-1}{i} \hat{\mathbf{R}}_{yy}^{(i-1)} + \frac{1}{iK} \mathbf{Y}_i \mathbf{Y}_i^H. \quad (58)$$

As the number of effective snapshots increases from  $K$  to  $iK$ , the FIM grows proportionally, leading to a monotonically decreasing CRLB.

To balance convergence speed and precision, a variable step-size strategy guided by the closed-form CRLB is adopted. Let  $\hat{\boldsymbol{\theta}}_{l,i-1}$  denote the estimated local DOA from the  $(i-1)$ -th iteration. The local search step sizes  $\Delta\boldsymbol{\theta}_i = [\Delta\theta_{\theta,i}, \Delta\phi_{\phi,i}]^T$  for the  $i$ -th iteration are designed as

$$\Delta\theta_{\theta,i} = \min \left( \sqrt{\text{CRLB}_{\theta}(\hat{\boldsymbol{\theta}}_{l,i-1}; iK)} \cdot \gamma^{r_i}, \Delta_{\max} \right), \quad (59)$$

$$\Delta\phi_{\phi,i} = \min \left( \sqrt{\text{CRLB}_{\phi}(\hat{\boldsymbol{\theta}}_{l,i-1}; iK)} \cdot \gamma^{r_i}, \Delta_{\max} \right), \quad (60)$$

where  $\gamma \in (0, 1)$  is a decay factor, and  $r_i$  is a refinement index. The CRLB is evaluated in the local array coordinate system.

The candidate set  $\Omega_{l,i}$  for the current iteration is defined around the previous local estimate as

$$\Omega_{l,i} = \left\{ \hat{\boldsymbol{\theta}}_{l,i-1} + \mathbf{d} \odot \Delta\boldsymbol{\theta}_i \mid \mathbf{d} \in \mathcal{D} \right\}, \quad (61)$$

where  $\mathcal{D}$  denotes the directional search space as follows

$$\mathcal{D} = \left\{ \begin{bmatrix} 0 \\ 0 \end{bmatrix}, \pm \begin{bmatrix} 1 \\ 0 \end{bmatrix}, \pm \begin{bmatrix} 0 \\ 1 \end{bmatrix} \right\}. \quad (62)$$

Subsequently, the updated local estimate is obtained by maximizing the spatial spectrum as follows

$$\hat{\boldsymbol{\theta}}_{l,i} = \arg \max_{\boldsymbol{\theta}_l \in \Omega_{l,i}} \mathbf{a}^H(\boldsymbol{\theta}_l) \hat{\mathbf{R}}_{yy}^{(i)} \mathbf{a}(\boldsymbol{\theta}_l). \quad (63)$$

Based on the newly obtained estimate, the search refinement index for the next iteration is updated as

$$r_{i+1} = \begin{cases} r_i + 1, & \text{if } \boldsymbol{\theta}_{l,i} = \boldsymbol{\theta}_{l,i-1}, \\ r_i, & \text{otherwise,} \end{cases} \quad (64)$$

where the initial index is set to  $r_1 = 0$ , and  $r_i$  is upper-bounded by  $r_{\max}$ .

The iterative search process terminates when the sequence of local DOA estimates converges, which is evaluated by

$$\left\| \hat{\boldsymbol{\theta}}_{l,i} - \hat{\boldsymbol{\theta}}_{l,i-1} \right\|_2 \leq \epsilon, \quad (65)$$

where  $\epsilon$  is a predefined small tolerance threshold. To prevent infinite loops in cases of severe noise or search stagnation, the algorithm is also forced to halt if the number of iterations reaches a maximum value  $I_{\max}$  or the refinement index exceeds its upper bound, i.e.,  $r_i > r_{\max}$ .

Let  $\hat{\boldsymbol{\theta}}_{l,\text{final}} = [\hat{\theta}_{l,\text{final}}, \hat{\phi}_{l,\text{final}}]^T$  denote the estimated local DOA upon convergence. The corresponding local direction vector is constructed and denoted as  $\hat{\mathbf{u}}_{l,\text{final}}$ .

To obtain the final DOA estimate in the global coordinate system, the local direction vector is mapped back using the previously fixed mechanical rotation matrix  $\mathbf{R}_{\text{init}}$  as follows

$$\hat{\mathbf{u}}_{\text{final}} = \mathbf{R}_{\text{init}} \hat{\mathbf{u}}_{l,\text{final}}. \quad (66)$$

Finally, the ultimate global DOA estimate, denoted as  $\hat{\boldsymbol{\theta}}_{\text{final}} = [\hat{\theta}_{\text{final}}, \hat{\phi}_{\text{final}}]^T$ , is extracted from the elements of  $\hat{\mathbf{u}}_{\text{final}}$  using the same inverse trigonometric mapping defined in Eq. (48) and Eq. (49).

### C. Computational Complexity Analysis

Now, the approximate computational complexities of the three rotatable array methods are analyzed. First, the complexity of the traditional RR-Root-MUSIC method is about  $C_{RR-\text{Root-MUSIC}} = \mathcal{O}(I(KL^2 + L^3))$  floating-point operations (FLOPs). For the proposed PRI, its computational complexity is approximated as  $C_{PRI} = \mathcal{O}(Q^2KL + KL^2 + L^3)$ . For the proposed PRI-IGSS, the iterative greedy search is executed upon the initialization of PRI. Accordingly, the complexity of the proposed PRI-IGSS is approximated as  $C_{PRI-IGSS} = C_{PRI} + \mathcal{O}(I(KL^2 + JL^2)) = \mathcal{O}(Q^2KL + KL^2 + L^3 + I(KL^2 + JL^2))$ , which is slightly higher than that of proposed PRI method. Generally, their complexities have a decreasing order as follows: RR-Root-MUSIC, PRI-IGSS, PRI.

## IV. SIMULATION RESULTS

In this section, we present simulation results to evaluate the performance of proposed PRI and PRI-IGSS methods and the corresponding CRLB as a performance benchmark. Simulation parameters are chosen as follows:  $N = M = 7$ ,  $P_t = 5$  dBm,  $\sigma^2 = 10$  dBm,  $\phi = 45^\circ$ ,  $\lambda = 0.125$ ,  $K = 512$ ,  $Q = 3$ ,  $\Psi_\alpha = \Psi_\beta = \{30^\circ, 90^\circ, 150^\circ\}$ . In our simulation, all results

are averaged over 2000 Monte Carlo realizations and RMSE is calculated to indicate the performance, which is given by

$$\text{RMSE} = \sqrt{\frac{1}{U} \sum_u (\theta_u - \theta)^2}, \quad (67)$$

where  $U$  denotes the times of Monte Carlo experiments.

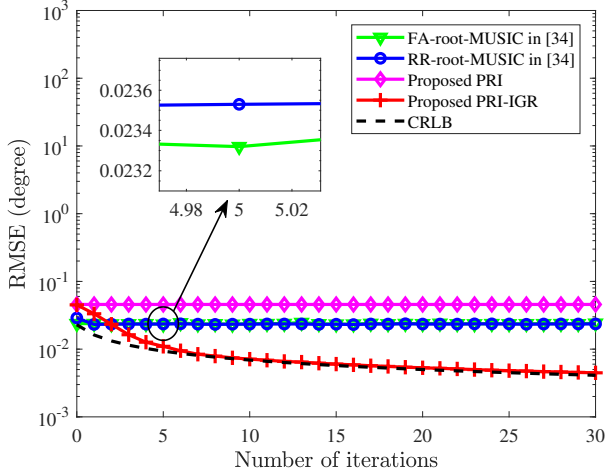


Fig. 5. Convergence curves of the proposed low-complexity methods for rotatable array when  $\theta = 5^\circ$ .

Fig. 5-7 illustrate the RMSE convergence curves of the proposed low-complexity PRI and PRI-IGR methods for three representative incident angles, i.e.,  $\theta = 5^\circ, 85^\circ, 175^\circ$ . The CRLB is also included as the theoretical performance benchmark. It is seen that the CRLB is continuously decreased over iterations due to the accumulation of sampling signals. While acceptable at  $\theta = 5^\circ$ , the conventional FA-Root-MUSIC method is completely disabled at large angles, i.e.,  $\theta = 85^\circ, 175^\circ$ , due to severe SNR attenuation. Although the RR-Root-MUSIC eventually converges, it requires multiple rotation iterations for larger boresight deflection angle

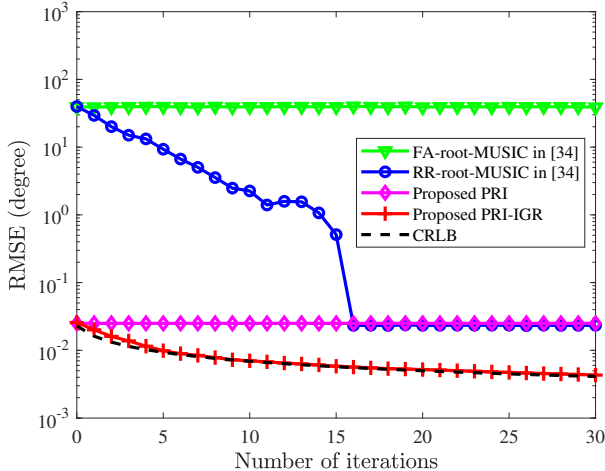


Fig. 6. Convergence curves of the proposed low-complexity methods for rotatable array when  $\theta = 85^\circ$ .

( $\theta = 85^\circ, 175^\circ$ ), resulting in high computational complexity, and still has a significant gap compared to the CRLB. By contrast, the proposed PRI method effectively improves the initialization accuracy by pre-rotation. On this basis, the PRI-IGSS method further improves the estimation through iterative greedy search with a continuous sampled signal accumulation process, leading to rapid convergence and performance that approaches the CRLB.

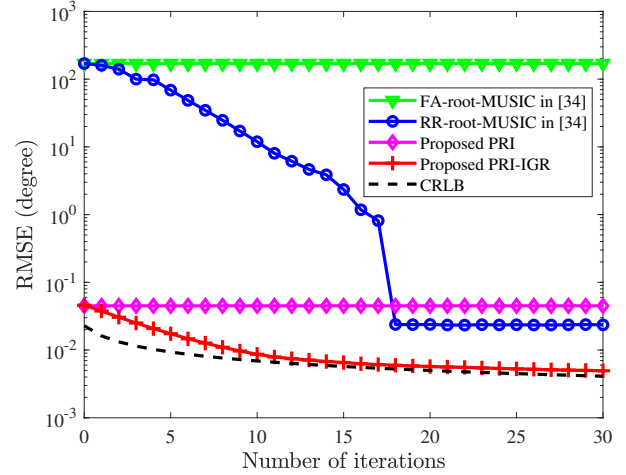


Fig. 7. Convergence curves of the proposed low-complexity methods for rotatable array when  $\theta = 175^\circ$ .

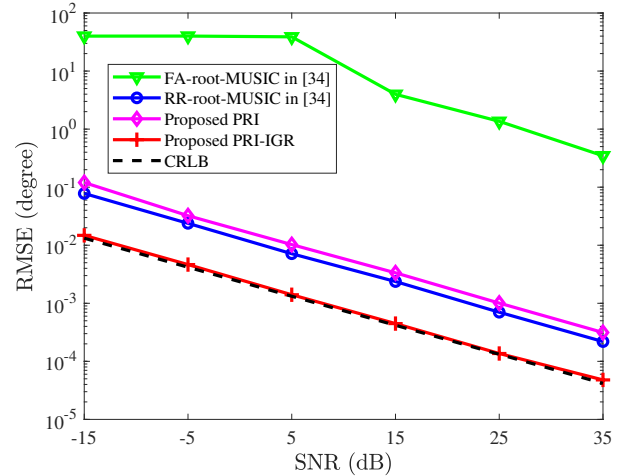


Fig. 8. RMSE versus SNR of the proposed methods when  $\theta = 85^\circ$ .

Fig. 8 shows the performance curves of RMSE versus SNR of the proposed methods with  $\theta = 85^\circ$ . Due to the directive antenna characteristics, the performance of the FA-Root-MUSIC is highly degraded. Although stable estimation is provided by the proposed PRI and traditional RR-Root-MUSIC respectively, and a noticeable gap from the CRLB is maintained. In contrast, the CRLB is perfectly achieved by the proposed PRI-IGSS across the entire SNR range from -15 dB to 35 dB. Consequently, one-order magnitude improvement in sensing accuracy is successfully achieved by PRI-IGSS compared with the PRI and RR-Root-MUSIC.

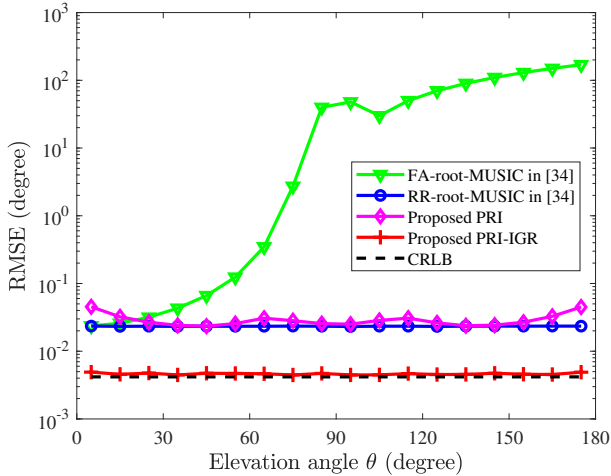


Fig. 9. RMSE versus the elevation angle  $\theta$  for the proposed methods when SNR = -5 dB.

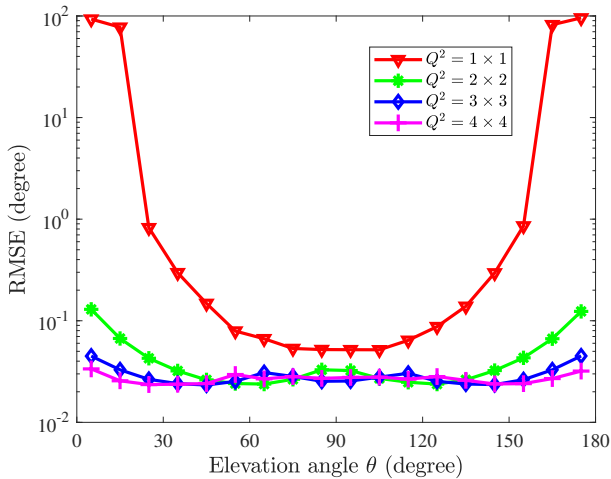


Fig. 10. RMSE versus the elevation angle  $\theta$  for the different number of candidate pre-rotation direction with SNR = 5 dB.

In Fig. 9, the RMSE performance versus the elevation angle  $\theta$  at a low SNR of -5 dB is evaluated. As  $\theta$  increases or the target deviates from the array boresight, a severe performance degradation is suffered by the FA-Root-MUSIC, particularly in off-boresight regions, i.e.,  $\theta > 80^\circ$ . In contrast, the PRI and PRI-IGSS improve the estimation accuracy by about three and four orders of magnitude, respectively. Moreover, over the entire angular range, the PRI-IGSS consistently outperforms the RR-Root-MUSIC by about one order of magnitude. These results show that PRI-IGSS still exhibits excellent spatial stability and excellent estimation performance even in extreme cases.

Fig. 10 plots the RMSE performance versus the elevation angle  $\theta$  for the different number of candidate pre-rotation directions at a SNR of -5 dB is evaluated. Based on equi-spaced rotation or sampling, the candidate angle sets for  $Q = 1, 2, 3$ , and 4 are respectively defined as  $\{90^\circ\}$ ,  $\{45^\circ, 135^\circ\}$ ,  $\{30^\circ, 90^\circ, 150^\circ\}$ , and  $\{22.5^\circ, 67.5^\circ, 112.5^\circ, 157.5^\circ\}$ . As illus-

trated, a negligible performance difference between  $Q = 3$  and  $Q = 4$  is observed. This implies that the main high-gain region of the array is sufficiently covered by the candidate set of  $Q = 3$ . Consequently, only marginal accuracy improvements are provided by further increasing  $Q$ , while the number of rotation is increased, i.e., from 9 to 16. Thus,  $Q = 3$  is verified as the optimal configuration to balance sensing precision and computational burden.

## V. CONCLUSIONS

In this paper, to address the critical challenges of high computational complexity and low time efficiency in practical rotatable array systems, we proposed a low-complexity enhanced direction-sensing framework with a pre-rotation operation, which will provide a good initial value for the following iterative sensing step and will speed up the convergent process. Furthermore, the corresponding CRLB was derived to provide a rigorous theoretical benchmark for the rotatable array model. The proposed framework is divided into three stages: first, a finite number of equal-space samplings are utilized to obtain a highly reliable initial estimate in the PRI stage. Subsequently, the array is rotated to the initial estimate direction. Finally, in the IGSS stage, a receive beamforming is performed on the candidate angles to find the maximum spatial spectrum, and by adopting a gradually decreasing search step size, the estimation accuracy is continuously improved. Crucially, the proposed PRI-IGSS method dramatically decreases the repeated use of EVD of Root-MUSIC to sensing the direction, which reduces the computational complexity. Through simulation and analysis, we found that the proposed PRI-IGSS can achieve the CRLB. Compared to the traditional FA-Root-MUSIC method, it improved the performance by up to four orders of magnitude at extreme elevation angles, for example,  $\theta > 80^\circ$ . Moreover, by exploiting continuous signal sampling accumulation, the proposed method exceeds the RR-Root-MUSIC approach by approximately one-order magnitude. Due to its merits in low complexity, rapid execution, and superior spatial accuracy, the PRI-IGSS method will be very suitable for the future Low-Altitude Wireless Network to implement a high-precision UAV direction sensing and perform a directive beam towards UAVs with an enhanced high energy efficiency.

## REFERENCES

- [1] G. Cheng, X. Song, Z. Lyu, and J. Xu, "Networked isac for low-altitude economy: Coordinated transmit beamforming and uav trajectory design," *IEEE Transactions on Communications*, vol. 73, no. 8, pp. 5832–5847, 2025.
- [2] H. Yuhong, D. Haiyu, C. Weiyang, K. Luting, D. Wei, L. Xin, L. Yang, W. Guizhen, and L. Liang, "Towards a low-altitude aerial intelligent network: Vision, challenges, and key technologies," *China Communications*, vol. 22, no. 9, pp. 1–21, 2025.
- [3] S. Gao, J. Yan, P. Huang, Z. Lu, M. Gong, L. Miao, G. Zhu, J. Liang, and L. Yang, "Integrated sensing, communication, and computation for low-altitude networks towards seamless connectivity and connected intelligence," *IEEE Internet of Things Magazine*, pp. 1–9, 2026.
- [4] X. Xia, Z. Yan, P. Huang, K. Xu, and W. Xie, "An ambiguity-function-assisted active sensing scheme for ofdm-based isac systems toward low-altitude airspace," *IEEE Internet of Things Journal*, vol. 12, no. 12, pp. 19471–19487, 2025.
- [5] Y. Yao, W. Xiao, P. Miao, G. Chen, H. Yang, C.-B. Chae, and K.-K. Wong, "Uav-rhs-enabled full-duplex isac covert system: Robust beamforming and trajectory optimization," *IEEE Transactions on Communications*, vol. 74, pp. 5637–5653, 2026.

- [6] Z. Xiao, L. Zhu, and X.-G. Xia, "Uav communications with millimeter-wave beamforming: Potentials, scenarios, and challenges," *China Communications*, vol. 17, no. 9, pp. 147–166, 2020.
- [7] F. Shu, Y. Qin, T. Liu, L. Gui, Y. Zhang, J. Li, and Z. Han, "Low-complexity and high-resolution doa estimation for hybrid analog and digital massive mimo receive array," *IEEE Transactions on Communications*, vol. 66, no. 6, pp. 2487–2501, 2018.
- [8] F. Shu, B. Shi, Y. Chen, J. Bai, Y. Li, T. Liu, Z. Han, and X. You, "A new heterogeneous hybrid massive mimo receiver with an intrinsic ability of removing phase ambiguity of doa estimation via machine learning," *IEEE Transactions on Machine Learning in Communications and Networking*, vol. 3, pp. 17–29, 2025.
- [9] X. Zhan, Z. Sun, F. Shu, Y. Chen, X. Cheng, Y. Wu, Q. Zhang, Y. Li, and P. Zhang, "Rapid phase ambiguity elimination methods for doa estimator via hybrid massive mimo receive array," *Chinese Journal of Electronics*, vol. 33, no. 1, pp. 175–184, 2024.
- [10] J. Bai, F. Shu, F. Zhou, Q. Zheng, B. Xu, B. Shi, Y. Chen, W. Zhang, and X. Wang, "Co-learning-aided multi-modal-deep-learning framework of passive doa estimators for a heterogeneous hybrid massive mimo receiver," *IEEE Journal of Selected Topics in Signal Processing*, vol. 19, no. 7, pp. 1448–1460, 2025.
- [11] Y. Chen, X. Zhan, F. Shu, Q. Jie, X. Cheng, Z. Zhuang, and J. Wang, "Two low-complexity doa estimators for massive/ultra-massive mimo receive array," *IEEE Wireless Communications Letters*, vol. 11, no. 11, pp. 2385–2389, 2022.
- [12] J. Zhang, G. Lu, L. Xiang, X. Ge, and D. W. K. Ng, "Energy minimization for uav-aided data collection along a fixed flight path with a directional antenna," *IEEE Transactions on Communications*, vol. 74, pp. 764–780, 2026.
- [13] M. Li, J. Xin, F. Shu, X. Wang, Y. Wu, and C. Pan, "Secure directional modulation with movable antenna array aided by ris," *IEEE Transactions on Vehicular Technology*, pp. 1–14, 2025.
- [14] J. Ren, Y. Tian, T. Wu, and W. Liu, "Fluid-antenna array enabled doa estimation for the hybrid analog-digital architecture with unknown nonuniform noise," in *2025 33rd European Signal Processing Conference (EUSIPCO)*, 2025, pp. 1447–1451.
- [15] L. Zhu, W. Ma, and R. Zhang, "Movable antennas for wireless communication: Opportunities and challenges," *IEEE Communications Magazine*, vol. 62, no. 6, pp. 114–120, 2024.
- [16] —, "Movable-antenna array enhanced beamforming: Achieving full array gain with null steering," *IEEE Communications Letters*, vol. 27, no. 12, pp. 3340–3344, 2023.
- [17] X. Zhang, W. Liu, J. Ren, C. Wang, H. Xing, Y. Shen, and S. Cui, "Movable-antenna empowered aav-enabled data collection over low-altitude wireless networks," *IEEE Transactions on Network Science and Engineering*, vol. 13, pp. 4506–4523, 2026.
- [18] W. K. New, K.-K. Wong, H. Xu, C. Wang, F. R. Ghadi, J. Zhang, J. Rao, R. Murch, P. Ramirez-Espinosa, D. Morales-Jimenez, C.-B. Chae, and K.-F. Tong, "A tutorial on fluid antenna system for 6g networks: Encompassing communication theory, optimization methods and hardware designs," *IEEE Communications Surveys & Tutorials*, vol. 27, no. 4, pp. 2325–2377, 2025.
- [19] W. K. New, K.-K. Wong, C. Wang, C.-B. Chae, R. Murch, H. Jafarkhani, and Y. Hao, "Fluid antenna systems: Redefining reconfigurable wireless communications," *IEEE Journal on Selected Areas in Communications*, vol. 44, pp. 1013–1044, 2026.
- [20] X. Shao, W. Mei, C. You, Q. Wu, B. Zheng, C.-X. Wang, J. Li, R. Zhang, R. Schober, L. Zhu, W. Zhuang, and X. Shen, "A tutorial on six-dimensional movable antenna for 6g networks: Synergizing positionable and rotatable antennas," *IEEE Communications Surveys & Tutorials*, vol. 28, pp. 3666–3709, 2026.
- [21] X. Pi, L. Zhu, H. Mao, and Z. Xiao, "Joint position and orientation optimization for 6dma enhanced multi-access point coordination," in *2025 IEEE Wireless Communications and Networking Conference (WCNC)*, 2025, pp. 1–6.
- [22] X. Pi, L. Zhu, H. Mao, Z. Xiao, X.-G. Xia, and R. Zhang, "6d movable antenna enhanced multi-access point coordination via position and orientation optimization," *IEEE Transactions on Wireless Communications*, vol. 25, pp. 915–930, 2026.
- [23] C. Huang, R. Mo, and C. Yuen, "Reconfigurable intelligent surface assisted multiuser miso systems exploiting deep reinforcement learning," *IEEE Journal on Selected Areas in Communications*, vol. 38, no. 8, pp. 1839–1850, 2020.
- [24] D. Rongen, S. Feng, L. Yongzhao, T. Yanqun, L. Jun, W. Yongpeng, and W. Jiangzhou, "Joint power allocation and beamforming for active ris-aided secure directional modulation network," *Science China Information Sciences*, vol. 68, p. 222301, 2025.
- [25] J. Jiang, F. Shu, X. Wang, K. Yang, C. Shen, Q. Zhang, D. Wang, and J. Wang, "Dof analysis and beamforming design for active ris-aided multi-user mimo wireless communication in low-rank channels," *Tsinghua Science and Technology*, 2025. [Online]. Available: <https://www.sciopen.com/article/10.26599/TST.2025.9010084>
- [26] F. Shu, Y. Teng, J. Li, M. Huang, W. Shi, J. Li, Y. Wu, and J. Wang, "Enhanced secrecy rate maximization for directional modulation networks via ris," *IEEE Transactions on Communications*, vol. 69, no. 12, pp. 8388–8401, 2021.
- [27] M. Li, F. Shu, Y. Si, R. Chen, C. Pan, and Y. Wu, "Near-field directional modulation for ris-aided movable antenna mimo systems with hardware impairments," *IEEE Transactions on Network Science and Engineering*, vol. 13, pp. 3944–3959, 2026.
- [28] M. Li, W. Gao, Q. Wu, F. Shu, C. Pan, and D. Wu, "Directional modulation design for uav assisted by ris with discrete phase shift," *IEEE Transactions on Green Communications and Networking*, vol. 10, pp. 172–186, 2026.
- [29] W. Xiao, Y. Yao, J. Yang, and X. Cheng, "Joint beamforming design for ris-enabled dfrc systems via multiobjective optimization," *IEEE Transactions on Vehicular Technology*, pp. 1–16, 2026.
- [30] Z. Zhang, Q. Wu, W. Chen, Y. Zhu, Z. Zheng, Y. Gao, and Q. Wu, "Ris-aided secure sensing for surveillance area coverage: Framework and algorithm design," *IEEE Journal on Selected Areas in Communications*, pp. 1–1, 2026.
- [31] X. Xiong, B. Zheng, W. Wu, W. Zhu, M. Wen, S. Lin, and Y. Zeng, "Intelligent rotatable antenna for integrated sensing, communication, and computation: Challenges and opportunities," *IEEE Wireless Communications*, vol. 33, no. 1, pp. 173–180, 2026.
- [32] B. Zheng, T. Ma, C. You, J. Tang, R. Schober, and R. Zhang, "Rotatable antenna enabled wireless communication and sensing: Opportunities and challenges," *IEEE Wireless Communications*, pp. 1–8, 2025.
- [33] X. Zhang, L. Xiang, J. Wang, X. Gao, D. W. K. Ng, and R. Schober, "Rotatable antenna array enabled uav mmwave massive mimo communication," *IEEE Transactions on Communications*, vol. 74, pp. 1219–1236, 2026.
- [34] J. Jiang, F. Shu, B. Deng, M. Li, J. Bai, Y. Wang, C. Pan, and J. Wang, "Rotatable antenna-array-enhanced direction-sensing for low-altitude communication network: Method and performance," 2025.
- [35] R. Gurney, *The Printing of Mathematics*. Toronto: University of Toronto Press, 1961, pp. 127–134.
- [36] Tuncer and T. Engin, "Classical and modern direction-of-arrival estimation," *Academic Press*, pp. 125–160, 2009.
- [37] A. Wang, L. Liu, and J. Zhang, "Low complexity direction of arrival (doa) estimation for 2d massive mimo systems," in *2012 IEEE Globecom Workshops*, 2012, pp. 703–707.
- [38] *Fundamentals of Statistical Signal Processing*. London: Springer London, 2006, pp. 83–182.
- [39] S. K. Sengijpta, "Fundamentals of statistical signal processing: Estimation theory," *Control Engineering Practice*, vol. 37, no. 4, pp. 465–466, 1994.